



**HAL**  
open science

# Equatorial noise emissions observed by the DEMETER spacecraft during geomagnetic storms

F. Němec, Michel Parrot, O. Santolík

► **To cite this version:**

F. Němec, Michel Parrot, O. Santolík. Equatorial noise emissions observed by the DEMETER spacecraft during geomagnetic storms. *Journal of Geophysical Research Space Physics*, 2016, 121 (10), pp.9744-9757. 10.1002/2016JA023145 . insu-01393999

**HAL Id: insu-01393999**

**<https://insu.hal.science/insu-01393999>**

Submitted on 21 Nov 2016

**HAL** is a multi-disciplinary open access archive for the deposit and dissemination of scientific research documents, whether they are published or not. The documents may come from teaching and research institutions in France or abroad, or from public or private research centers.

L'archive ouverte pluridisciplinaire **HAL**, est destinée au dépôt et à la diffusion de documents scientifiques de niveau recherche, publiés ou non, émanant des établissements d'enseignement et de recherche français ou étrangers, des laboratoires publics ou privés.

## RESEARCH ARTICLE

10.1002/2016JA023145

## Equatorial noise emissions observed by the DEMETER spacecraft during geomagnetic storms

## Key Points:

- During periods of enhanced geomagnetic activity equatorial noise emissions penetrate down to DEMETER altitudes (700 km)
- Daytime wave activity within 20 degrees from the equator is significantly enhanced; the nighttime wave activity increase is weaker
- Wave intensity increases by as much as 3 orders of magnitude during severely disturbed periods

## Correspondence to:

F. Němec,  
frantisek.nemec@gmail.com

## Citation:

Němec, F., M. Parrot, and O. Santolík (2016), Equatorial noise emissions observed by the DEMETER spacecraft during geomagnetic storms, *J. Geophys. Res. Space Physics*, 121, 9744–9757, doi:10.1002/2016JA023145.

Received 7 JUL 2016

Accepted 27 SEP 2016

Accepted article online 1 OCT 2016

Published online 19 OCT 2016

F. Němec<sup>1</sup>, M. Parrot<sup>2</sup>, and O. Santolík<sup>1,3</sup><sup>1</sup>Faculty of Mathematics and Physics, Charles University in Prague, Prague, Czech Republic, <sup>2</sup>LPC2E/CNRS, Orléans, France,<sup>3</sup>Institute of Atmospheric Physics, Czech Academy of Sciences, Prague, Czech Republic

**Abstract** Equatorial noise emissions are electromagnetic waves routinely observed in the equatorial region of the inner magnetosphere at frequencies between the proton cyclotron frequency and the lower hybrid frequency. Their observations are, however, typically limited to radial distances larger than about  $2R_E$ . We use the data measured by the low-altitude DEMETER spacecraft (altitude of about 700 km) to confirm that during periods of enhanced geomagnetic activity, these emissions penetrate down to low radial distances and eventually become a dominant wave emission close to the proton cyclotron frequency in the equatorial region. Wave data obtained during six intense geomagnetic storms ( $Dst < -100$  nT) are analyzed. It is shown that during the analyzed time intervals, the daytime wave activity within about  $20^\circ$  from the geomagnetic equator is significantly enhanced, while the nightside wave activity shows a weaker increase at lower frequencies. Multicomponent wave data allow us to determine dayside wave propagation parameters. It is shown that the waves are nearly linearly polarized and their wave vector directions are almost perpendicular to the ambient Earth's magnetic field, as it has been previously observed for equatorial noise emissions. Finally, we analyze the dependence of the equatorial wave intensity at the proton cyclotron frequency on  $Dst$  and  $AE$  geomagnetic indices, and we demonstrate that the dayside wave intensity increases by as much as 3 orders of magnitude during severely disturbed periods.

## 1. Introduction

Equatorial noise (EN) emissions are electromagnetic waves observed in the equatorial region of the inner magnetosphere at frequencies between the proton cyclotron frequency and the lower hybrid frequency. They are rather routinely observed at radial distances between about 3 and 6 Earth radii ( $R_E$ ) and within about  $5^\circ$  from the geomagnetic equator [Santolík et al., 2004; Němec et al., 2005; Ma et al., 2013; Hrbáčková et al., 2015], but they can occasionally occur at significantly larger radial distances [Hrbáčková et al., 2015] and latitudes [Tsurutani et al., 2014; Zhima et al., 2015]. These emissions are important for the dynamics of energetic electrons in the radiation belts [Horne et al., 2007; Bortnik and Thorne, 2010; Bortnik et al., 2015; Ma et al., 2016; Shprits, 2016].

Although the emissions originally appeared as a noise in low-resolution data [Russell et al., 1970], an analysis of high-resolution frequency-time spectrograms revealed that they are in fact composed by a system of many harmonic spectral lines [Gurnett, 1976] related to the proton cyclotron frequency in the source region. These are generated by instabilities of ring-like proton distributions functions. The generation mechanism appears to be theoretically rather well understood [McClements et al., 1994; Horne et al., 2000; Liu et al., 2011; Chen et al., 2011, 2016], and there is also an experimental evidence of the ring-like proton distribution functions observed in association with the waves [Perraut et al., 1982; Boardsen et al., 1992; Xiao et al., 2013; Ma et al., 2014; Balikhin et al., 2015].

Once generated, the emissions propagate in the extraordinary mode nearly perpendicular to the ambient Earth's magnetic field [Kasahara et al., 1994; Walker et al., 2015; Boardsen et al., 2016]. This directly implies why EN emissions are limited to frequencies below the lower hybrid frequency [Stix, 1992]. Magnetic field fluctuations of the emissions are nearly linearly polarized along the ambient Earth's magnetic field, and the electric field fluctuations are elliptically polarized in the equatorial plane. The major polarization axis of the electric field polarization ellipse is oriented along the wave vector direction [Laakso et al., 1990], which can be used to determine the propagation direction [Santolík et al., 2002]. The emissions were observed both inside and outside the plasmasphere. EN emissions observed outside the plasmasphere typically have higher

**Table 1.** Overview of Electromagnetic Emissions Reported in DEMETER Spacecraft Data During Main and Recovery Phases of Magnetic Storms at Different Latitudes and Frequency Ranges<sup>a</sup>

Frequency	Location	Nature of the Emissions	References
ULF	low latitudes	EMIC waves	<i>Piša et al.</i> [2015]
ELF	equator	EN emissions	<i>Santolík et al.</i> [2016]
ELF	equator	LH turbulence	<i>Berthelier et al.</i> [2008] <i>Malingre et al.</i> [2008]
ELF	trough	harmonic emissions	<i>Parrot et al.</i> [2006b]
ELF	trough and high latitudes	bursty emissions	<i>Parrot et al.</i> [2014]
ELF/VLF	low and middle latitudes	QP emissions	<i>Hayosh et al.</i> [2013, 2014, 2016]
ELF/VLF	midlatitudes	banded emissions	<i>Colpitts et al.</i> [2012]
ELF/VLF	all latitudes	overall intensity	<i>Zhima et al.</i> [2014]
MF	high latitudes	bursty emissions	<i>Broughton et al.</i> [2014]
MF	high latitudes	AKR-like emissions	<i>Parrot and Berthelier</i> [2012]

<sup>a</sup>EMIC stands for electromagnetic ion cyclotron, EN for equatorial noise, QP for quasiperiodic, LH for lower hybrid, AKR for auroral kilometric radiation.

frequencies and are more intense than those observed in the plasmasphere [Ma et al., 2013; Němec et al., 2015a]. Further, the propagation pattern inside and outside the plasmasphere appears to be rather different. While the emissions propagate with a broad distribution of wave vectors centered in the azimuthal direction in the plasma trough, their propagation can have principally any direction inside the plasmasphere [Němec et al., 2013].

This suggests that for a large range of azimuthal orientations of the wave vector, the waves can be efficiently trapped inside the plasmasphere, being reflected both at low and large radial distances [Chen and Thorne, 2012]. They may thus propagate over a broad region of magnetic local time (MLT) [Xiao et al., 2012]. In order to propagate down to low altitudes, the wave vectors of the emissions would have to be almost in the meridional plane, i.e., oriented nearly toward the Earth [Chen and Thorne, 2012]. This simplified theoretical assertion has been recently demonstrated using a ray tracing simulation by Santolík et al. [2016]. This study also used the data of the DEMETER spacecraft recorded during disturbed geomagnetic activity to demonstrate that EN emissions can penetrate down to low altitudes. It appears that they could be rather significant, in particular during periods of enhanced geomagnetic activity. Quasiperiodic events observed by DEMETER close to the geomagnetic equator have propagation parameters expected for EN [Hayosh et al., 2016], possibly corresponding to modulated EN observed formerly at larger radial distances [Boardsen et al., 2014; Fu et al., 2014; Němec et al., 2015b].

These examples, together with previous studies of the data recorded by the low-altitude satellite DEMETER, have shown that during main and recovery phases of a magnetic storm, the ionosphere is invaded at different latitudes by a dramatic variety of waves at various frequencies. An overview of these waves is shown in Table 1. Additionally, there are other emissions in the lower part of the ultralow frequency (ULF, up to about 15 Hz) range not observed by DEMETER [see, e.g., Menk, 2011].

In the present study we focus on electromagnetic waves observed by DEMETER in the equatorial region during six strong isolated geomagnetic storms. We demonstrate that EN emissions routinely penetrate down to 700 km altitudes during these periods. They eventually become dominant in a given range of geomagnetic latitudes and frequencies. DEMETER wave measurements are described in section 2. Section 3 presents the obtained results. These are discussed in section 4, and they are summarized in section 5.

## 2. Data Set

DEMETER spacecraft was a low-altitude spacecraft which operated between June 2004 and December 2010. The spacecraft orbit was circular at an altitude of about 700 km. Further, it was nearly Sun synchronous; i.e., the spacecraft was always located either close to the local noon (about 10:30 LT) or close to the local midnight (about 22:30 LT). The measured data can be thus effectively divided into those measured during the daytime parts of DEMETER orbits and those measured during the nighttime parts of the orbits. An exact

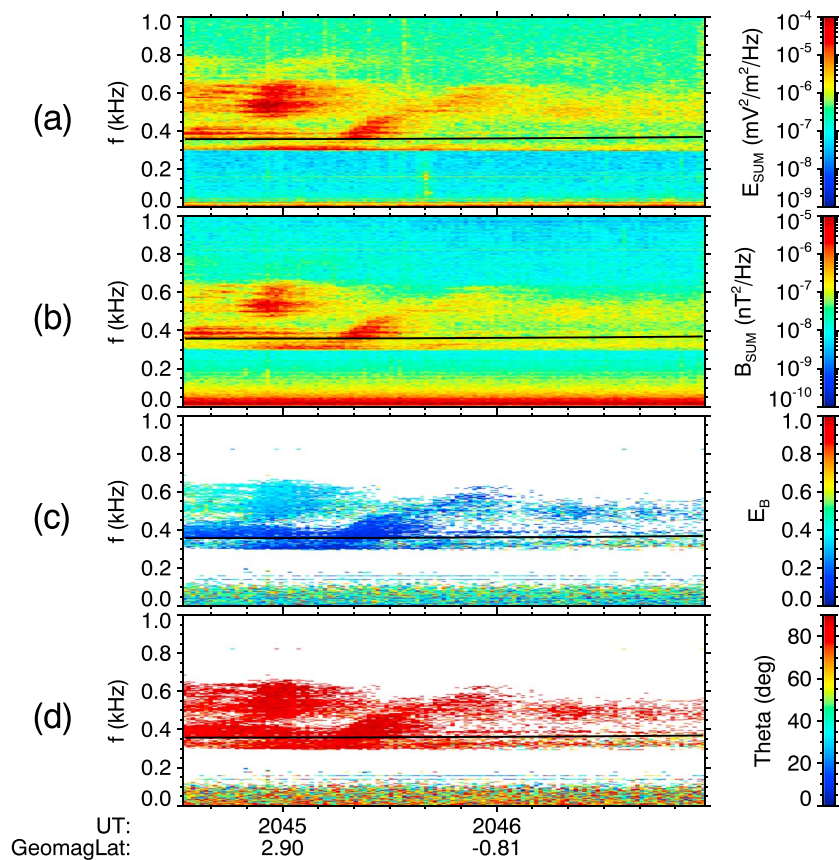


**Figure 1.** Example of an equatorial noise event measured by the DEMETER spacecraft. The data were obtained on 12 September 2005 between about 20:44:30 UT and 20:47:00 UT. (a) Frequency-time spectrogram of power spectral density of electric field fluctuations. (b) Frequency-time spectrogram of power spectral density of magnetic field fluctuations. (c) Frequency-time plot of ellipticity of magnetic field fluctuations. (d) Frequency-time plot of polar angle of wave vector direction with respect to the ambient magnetic field. The nearly horizontal black curve shown in individual panels corresponds to the proton cyclotron frequency at the spacecraft location. The emissions are limited to frequencies larger than the  $L = 0$  cutoff frequency (see text).

distribution of MLTs at which DEMETER took measurements is shown in Figure 1 of *Němec et al.* [2010]. During about 6.5 years of operation, DEMETER performed continuous wave measurements at geomagnetic latitudes lower than about  $65^\circ$ . For technical reasons, no measurements were performed in the polar regions. In the continuous Survey mode wave measurements in the very low frequency (VLF, up to 20 kHz) range consisted of a power spectrum of one electric and one magnetic field component. The time resolution of these measurements was about 2 s, and the frequency resolution was about 20 Hz. During the so-called Burst mode, which is active only during specifically selected time intervals, more precise data are measured in addition to the aforementioned Survey mode data. In the VLF range, the Burst mode data consist of waveforms of one electric and one magnetic field component measured with the sampling frequency of 40 kHz. Moreover, in the extra low frequency (ELF, up to 1250 Hz) range, waveforms of all six electromagnetic field components are measured with the sampling frequency of 2500 Hz. These multicomponent wave measurements allow us to perform a detailed wave analysis [*Santolik et al.*, 2006], i.e., to determine wave polarization and propagation properties. A more detailed description of electric and magnetic field measurements performed by the DEMETER spacecraft was given by *Berthelier et al.* [2006] and *Parrot et al.* [2006a], respectively.

### 3. Results

An example of an EN event observed by the DEMETER spacecraft is shown in Figure 1. Figures 1a and 1b show frequency-time spectrograms of power spectral density of electric and magnetic field fluctuations, respectively. The data were measured on 12 September 2005 between about 20:44:30 UT and 20:47:00 UT.

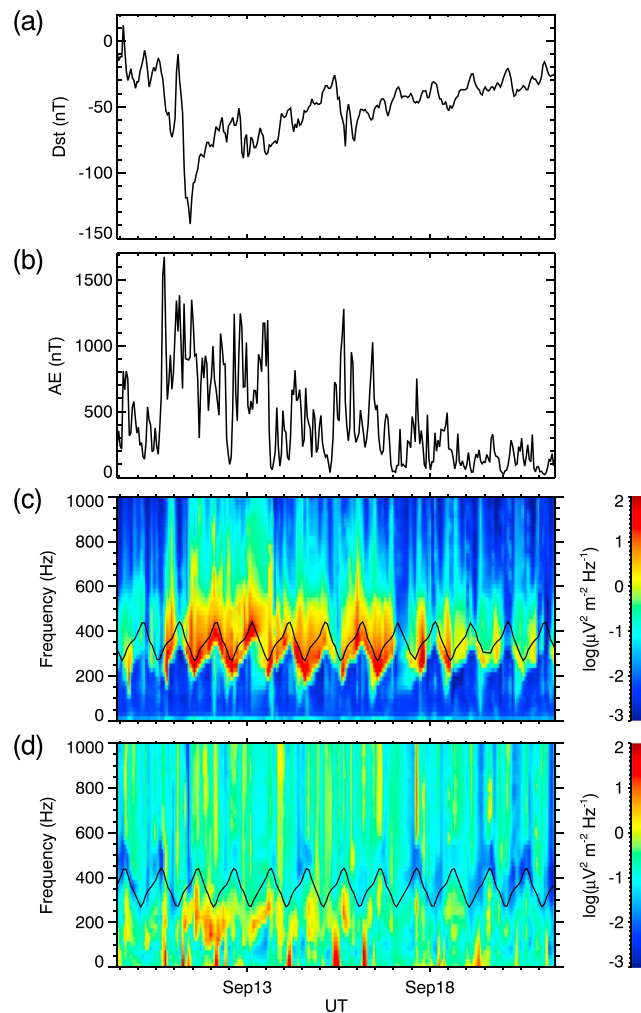


**Figure 2.** Evolution of geomagnetic indices and wave intensity during a geomagnetic storm which occurred in September 2005. (a) *Dst* index as a function of time. The minimum value of *Dst* was  $-139$  nT on 11 September 2005 at 10:30 UT. (b) *AE* index as a function of time. (c) Frequency-time plot of mean daytime power spectral density of electric field fluctuations at geomagnetic latitudes within  $5^\circ$  from the geomagnetic equator. The overplotted black curve shows the minimum of the proton cyclotron frequency during each equatorial crossing of the DEMETER spacecraft. (d) The same as Figure 2c but during the nighttime.

EN emissions are the intense waves best pronounced in the left part of the plotted time interval at frequencies between about 0.4 and 0.6 kHz. The nearly horizontal black curve shows the proton cyclotron frequency at the spacecraft location. The emissions are limited to frequencies larger than the cutoff frequency, which corresponds to the frequency of the  $L = 0$  cutoff. This cutoff is related to the proton cyclotron frequency and the plasma composition, and it is generally below the proton cyclotron frequency [Gurnett and Burns, 1968; Santolik *et al.*, 2006, 2016]. This is well consistent with the linearly polarized waves in Figure 1 extending down to frequencies of about 300 Hz, i.e., to frequencies by about 50 Hz lower than the local proton cyclotron frequency. An important feature identifiable in Figures 1a and 1b is the fine line structure of the emissions. This is expected for EN emissions, consistent with their generation mechanism. Moreover, it can be seen that the emissions are not continuous in time, but rather, their intensity exhibits a modulation of the wave intensity.

As the data were measured during the Burst mode, multicomponent data are available, and a detailed wave analysis can be performed [Santolik *et al.*, 2006]. Figure 1c shows a frequency-time plot of the ellipticity of magnetic field fluctuations determined using the Singular Value Decomposition (SVD) method by Santolik *et al.* [2003]. It is equal to the ratio of minor to major polarization axes; i.e., ellipticity values equal to 1 correspond to a circular polarization, and ellipticity values equal to 0 correspond to linear polarization. This is the expected situation for EN emissions [Santolik *et al.*, 2004], as they propagate in the extraordinary mode

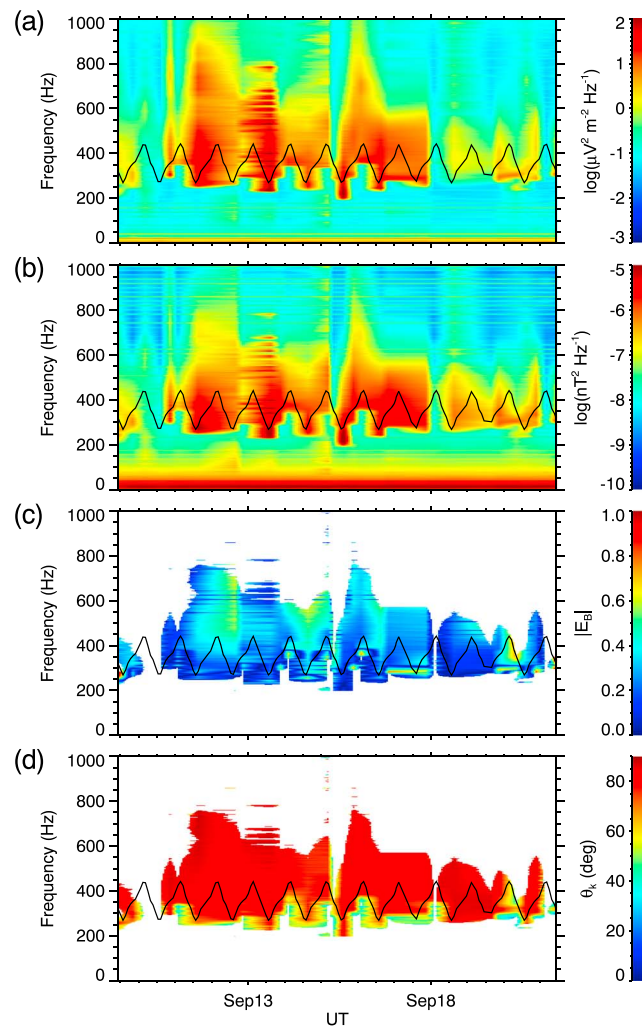
nearly perpendicular to the ambient magnetic field. It can be seen that the values of ellipticity obtained for the frequency-time interval with EN emissions are indeed close to 0. Note that the values of ellipticity were evaluated only for frequency-time intervals with power spectral density of magnetic field fluctuations larger than  $10^{-7} \text{ nT}^2 \text{ Hz}^{-1}$ , in order to prevent the calculation in frequency-time intervals dominated by noise. Frequency-time plot of the polar angle of wave vector direction with respect to the ambient magnetic field is shown in Figure 1d. This was determined as the direction perpendicular to the plane of the magnetic field fluctuations, again using the SVD method of Santolik *et al.* [2003]. The same intensity threshold for power spectral density of magnetic field fluctuations as in Figure 1c was used. It can be seen that the values of wave normal angles obtained for EN emissions are close to  $90^\circ$ , as expected.

EN emissions penetrating down to the low altitudes of the DEMETER spacecraft appear to be a very rare phenomenon [Santolik *et al.*, 2016]. However, at times of an enhanced geomagnetic activity, their occurrence rate substantially increases, and they eventually become the most intense wave emission in a given range of frequencies and geomagnetic latitudes. The importance of the enhanced geomagnetic activity for the EN occurrence at low altitudes is demonstrated in Figure 2. It shows the evolution of geomagnetic indices and wave intensity in the equatorial region during a geomagnetic storm which occurred in September 2005. Figure 2a shows the time variation of the *Dst* index. The *Dst* index reached a minimum value of  $-139 \text{ nT}$  on 11 September 2005 at about 10:30 UT. The time interval ranging from 2 days before the *Dst* minimum to 10 days after the *Dst* minimum is plotted. Figure 2b shows the time variation of the *AE* index. It can be seen that the *AE* index is increased at the time of the geomagnetic storm, as expected.

Figures 2c and 2d show frequency-time plots of mean power spectral density of electric field fluctuations at geomagnetic latitudes within  $5^\circ$  from the geomagnetic equator during the daytime and during the nighttime, respectively, using the Survey mode data set. The intensity values obtained for individual equatorial crossings were interpolated using an exponential interpolation to provide an apparently continuous data coverage. The latitudinal threshold of  $5^\circ$  was used as EN emissions are known to occur in a limited region close to the geomagnetic equator. The used value is a reasonable compromise between too low latitudinal range (which would result in not enough data and, moreover, would cause problems related to min-B equator being not exactly the same as the dipole magnetic equator) and too large latitudinal range (which would result in including latitudinal regions where EN emissions do not occur). The overplotted black curves show the minimum value of the proton cyclotron frequency at the spacecraft location during each DEMETER equatorial crossing. Note that in the dipole magnetic field approximation the minimum proton cyclotron frequency should be the same for all equatorial crossings. However, as the real magnetic field configuration at DEMETER altitudes differs quite significantly from a dipole, the minimum proton cyclotron frequency depends on the geomagnetic longitude.

Figure 2c shows that the power spectral density of electric field fluctuations measured close to the geomagnetic equator during the daytime significantly increases around the time of the *Dst* minimum, and it remains enhanced principally during the entire recovery phase. Eventually, the level of electric field fluctuations returns back to its prestorm values at the end of the plotted time interval. The frequencies where the power spectral densities are increased exhibit a clear lower cutoff. The frequency of this cutoff is lower than the proton cyclotron frequency, but it roughly follows its evolution, consistent with the expected behavior of the  $L = 0$  cutoff. The behavior of the power spectral density of electric field fluctuations close to the geomagnetic equator during the nighttime is rather different, as demonstrated in Figure 2d. The wave activity is also slightly increased, but the waves mostly occur at frequencies well below the proton cyclotron frequency. This is consistent with nighttime observations of Santolik *et al.* [2016], who also observed the waves well below the local proton cyclotron frequency.

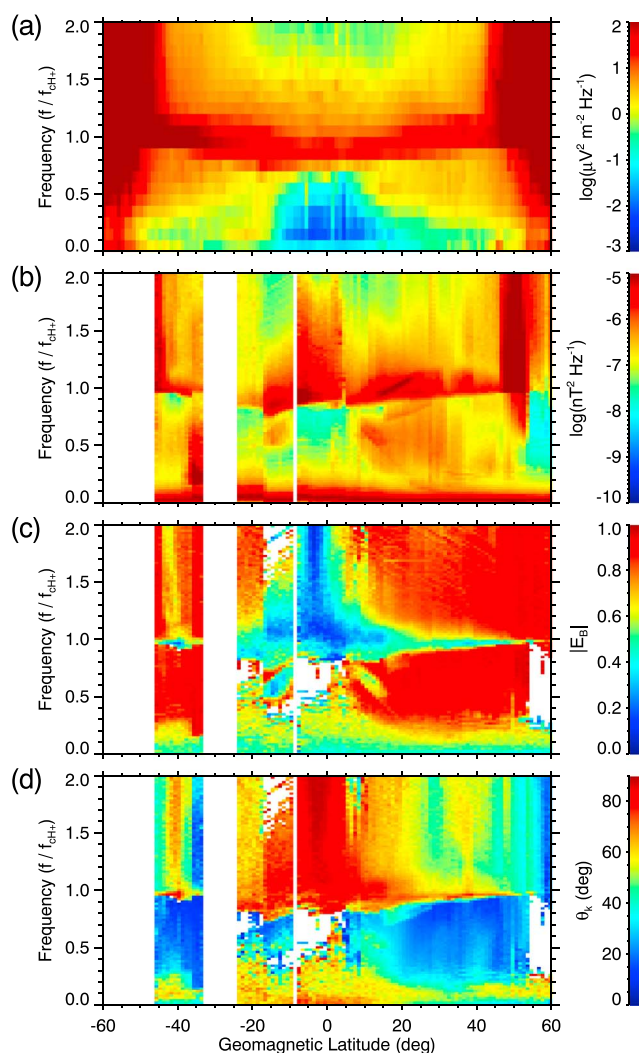
At frequencies lower than  $1250 \text{ Hz}$ , i.e., in the frequency range that we are interested in, DEMETER provided multicomponent waveform measurements. Although these were limited to specific time intervals, they are very important, as they allow us to determine detailed wave properties [Santolik *et al.*, 2003]. The results of such an analysis are shown in Figure 3 using a similar format as in Figure 2. The average wave parameters within  $5^\circ$  from the geomagnetic equator are plotted as a function of frequency (ordinate) and time (abscissa). Only the data measured during daytime half-orbits were used. Figures 3a–3d show the plots of power spectral density of electric field fluctuations, power spectral density of magnetic field fluctuations, ellipticity of magnetic field fluctuations, and polar angle of wave vector direction, respectively. Note that as the Burst mode is active only during specific time intervals, the data coverage in Figure 3 is significantly worse than the data



**Figure 3.** Frequency-time plots of wave propagation parameters determined using multicomponent Burst mode data within 5° from the geomagnetic equator during the daytime. (a) Power spectral density of electric field fluctuations, (b) power spectral density of magnetic field fluctuations, (c) ellipticity of magnetic field fluctuations, and (d) polar angle of wave vector direction. The black curves show the minimum proton cyclotron frequency during each equatorial crossing of the DEMETER spacecraft.

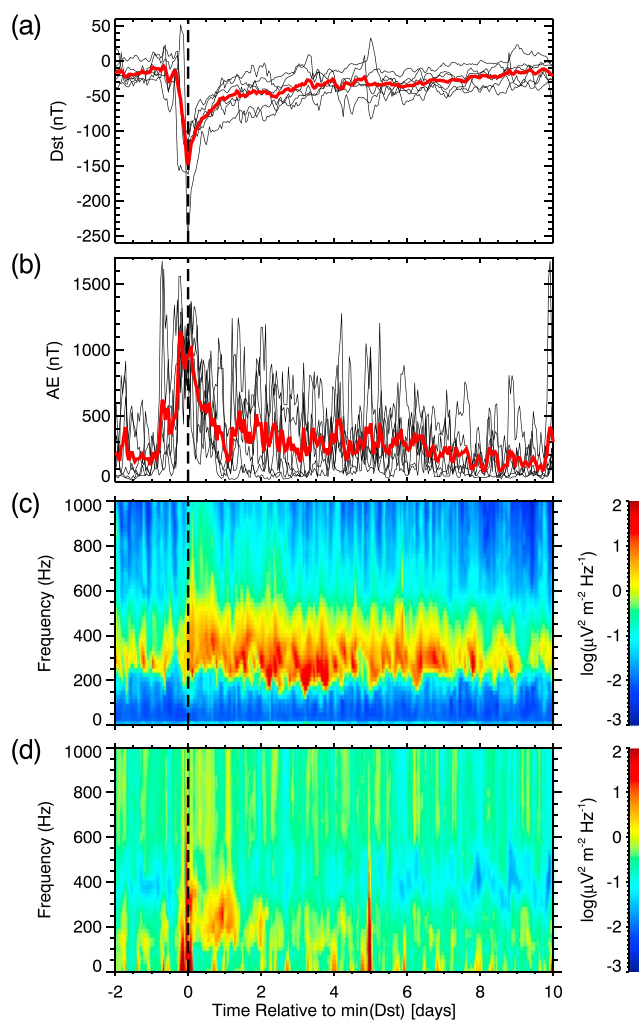
coverage in Figure 2. Altogether, there were 30 DEMETER daytime half-orbits with Burst mode coverage within 5° from the geomagnetic equator. These were interpolated to provide an apparently continuous data coverage in Figure 3. An exponential interpolation of the wave intensity and linear interpolation of wave propagation parameters in individual frequency bins was used. The ellipticity of magnetic field fluctuations and polar angle of wave vector direction were determined only for frequency-time intervals when the power spectral density of magnetic field fluctuations was larger than  $10^{-7}$  nT<sup>2</sup> Hz<sup>-1</sup>. The overplotted black curves in individual panels correspond to the minimum of proton cyclotron frequency during each equatorial crossing of the DEMETER spacecraft.

Figure 3a effectively corresponds to Figure 2c, while Figure 3b shows the analogous plot obtained for the power spectral density of magnetic field fluctuations. However, these figures were calculated using the Burst mode data only; i.e., they demonstrate the worse Burst mode coverage as compared to the continuous coverage of the Survey mode. Figure 3c shows that the ellipticity of magnetic field fluctuations of the observed emissions is rather low, as expected for EN emissions. Correspondingly, the wave normal angle depicted in Figure 3d is generally close to 90°, corresponding to the situation of wave vector perpendicular to the ambient magnetic field. The wave properties of the observed emissions are thus consistent with those expected for EN emissions, demonstrating that the detected wave activity can be really attributed to EN.



**Figure 4.** Frequency-geomagnetic latitude plots of wave parameters during the daytime. The data obtained within 2 days after the *Dst* minimum, i.e., between 11 September 2005 10:30 UT and 13 September 2005 10:30 UT were used. The frequency (ordinate) is normalized by the proton cyclotron frequency at the spacecraft location. (a) Results obtained for power spectral density of Survey mode electric field data. (b) Results obtained for power spectral density of Burst mode magnetic field data. (c) Results obtained for ellipticity of magnetic field fluctuations evaluated using the multicomponent Burst mode data. (d) Results obtained for polar angle of wave vector direction evaluated using the multicomponent Burst mode data.

It is of interest to determine the latitudinal and frequency range where EN emissions dominate over other electromagnetic wave activity. This is done in Figure 4, which shows frequency-geomagnetic latitude plots of relevant wave parameters. The data obtained within 2 days after the *Dst* minimum, i.e., between 11 September 2005 10:30 UT and 13 September 2005 10:30 UT were used. The frequency (ordinate) is normalized by the proton cyclotron frequency at the spacecraft location. This attempts to account for the effect of the low-frequency threshold of the observed emissions, which approximately follows the local proton cyclotron frequency. Nevertheless, this normalization means that the same values of the normalized frequencies correspond at larger latitudes to higher absolute frequencies. The normalized frequency-geomagnetic latitude plot of power spectral density of electric field fluctuations is shown in Figure 4a. It was constructed using the Survey mode data in order to obtain the best available coverage. For comparison, Figure 4b shows a normalized frequency-geomagnetic latitude plot of power spectral density of magnetic field fluctuations obtained using the Burst mode data. The Burst mode data were subsequently used to calculate detailed wave parameters in Figures 4c and 4d. These show the normalized frequency-geomagnetic latitude plots of the ellipticity of magnetic field fluctuations and of the polar angle of wave vector direction, respectively.



**Figure 5.** Analogous to Figure 2 but for all six analyzed geomagnetic storms using the superposed epoch analysis. The time zero, marked by vertical dashed lines, corresponds to the times of minimum  $Dst$  values. Variations of (a)  $Dst$  and (b)  $AE$  indices are shown. The black curves correspond to variations during the six individual geomagnetic storms. The red curves show the average variations. Variations of mean power spectral density of electric field fluctuations (c) during the daytime and (d) during the nighttime are shown.

Several regions with an intense wave activity can be identified in Figure 4. The frequency-latitude interval important for this paper, i.e., the frequency-latitude interval dominated by dayside EN emissions, is the frequency-latitude interval located at the geomagnetic equator and at normalized frequencies larger than about 1. The waves in this frequency-latitude interval are characterized by values of ellipticity close to 0 and wave normal angles close to  $90^\circ$ , as expected. Other regions of enhanced wave activity can be identified at larger geomagnetic latitudes. These waves are, however, nearly circularly polarized (note that we do not distinguish between the left-handed and right-handed polarization in the plot), and they propagate at lower wave normal angles.

Having demonstrated that EN emissions can efficiently penetrate down to DEMETER altitudes during a selected geomagnetic storm, it is of interest to investigate whether an analogous situation occurs also for other geomagnetic storms. In order to do so, we have investigated all major isolated storms which occurred during the lifetime of the DEMETER mission. Specifically, we focused on geomagnetic storms during which the  $Dst$  index decreased to less than  $-100$  nT. We further required no other geomagnetic storm to occur in a time window between 2 days before the  $Dst$  minimum and 10 days after the  $Dst$  minimum. This left us with six geomagnetic storms for which the DEMETER data were available. The minimum  $Dst$  values of these storms were  $-247$  nT,  $-113$  nT,  $-106$  nT,  $-122$  nT,  $-139$  nT, and  $-162$  nT. These minimum  $Dst$  values occurred on 15 May 2005, 30 May 2005, 13 June 2005, 31 August 2005, 11 September 2005, and 15 December 2006, respectively.

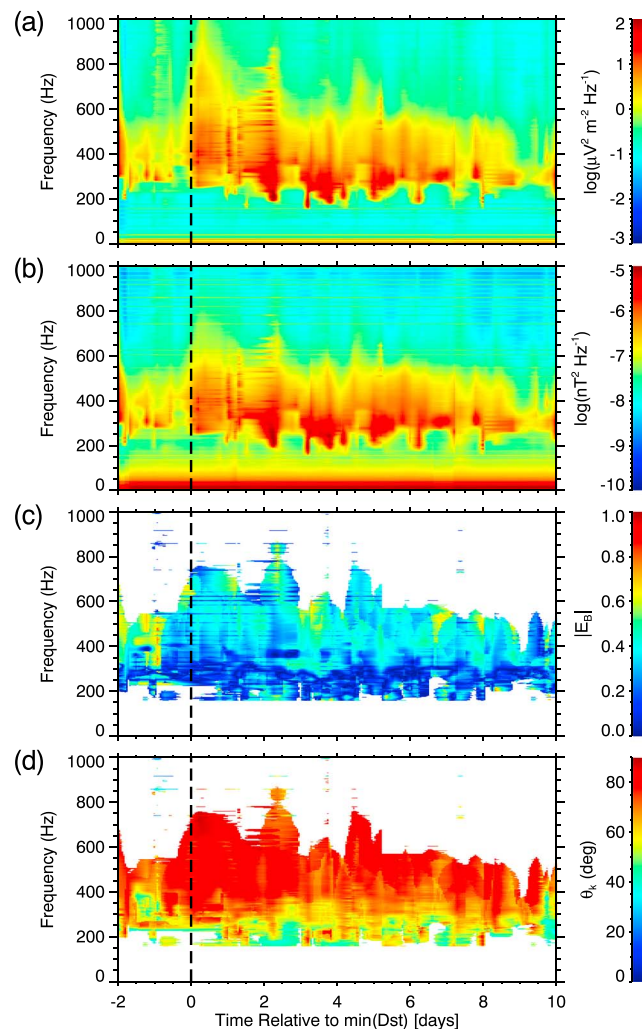


**Figure 6.** Analogous to Figure 3 but for all six analyzed geomagnetic storms using the superposed epoch analysis. The time zero, marked by vertical dashed lines, corresponds to the times of minimum *Dst* values.

Note that the largest storm which occurred during the DEMETER lifetime (November 2004,  $-374$  nT) is not included, as it exhibits a secondary *Dst* minimum, and it cannot be thus considered as isolated. The available data were, nevertheless, checked, and the wave activity in the equatorial region was found to be significantly increased (not shown), consistently with the presented results. It is, however, noteworthy, that during this extreme geomagnetic storm a significant wave activity increase was observed also during the nighttime.

In order to analyze systematic variations of investigated parameters during these six storms, we have used a superposed epoch analysis. The results obtained for individual storms were overlapped over each other, using the times of the *Dst* minima as “time zero.” Variations of the mean values of investigated parameters as a function of time relative to the time zero were then investigated, using the time window from  $-2$  to  $+10$  days.

The results obtained by the superposed epoch analysis method are shown in Figure 5. The format of the figure corresponds to the format of Figure 2. Figure 5a shows the time variation of *Dst* index during the six analyzed geomagnetic storms by the black curves. The red curve corresponds to the mean time dependence of the *Dst* index. The same representation is used in Figure 5b to depict the variation of the *AE* index. Figures 5c and 5d show the evolution of the mean value of power spectral density of electric field fluctuations within  $5^\circ$  from the geomagnetic equator during the daytime and during the nighttime, respectively. It can be seen that the evolution of the average wave intensity obtained using the superposed epoch analysis is similar to the aforementioned variation obtained for the selected geomagnetic storm. Specifically, the wave intensity during the daytime (Figure 5c) is significantly enhanced at the time of the *Dst* minimum, and it remains increased for

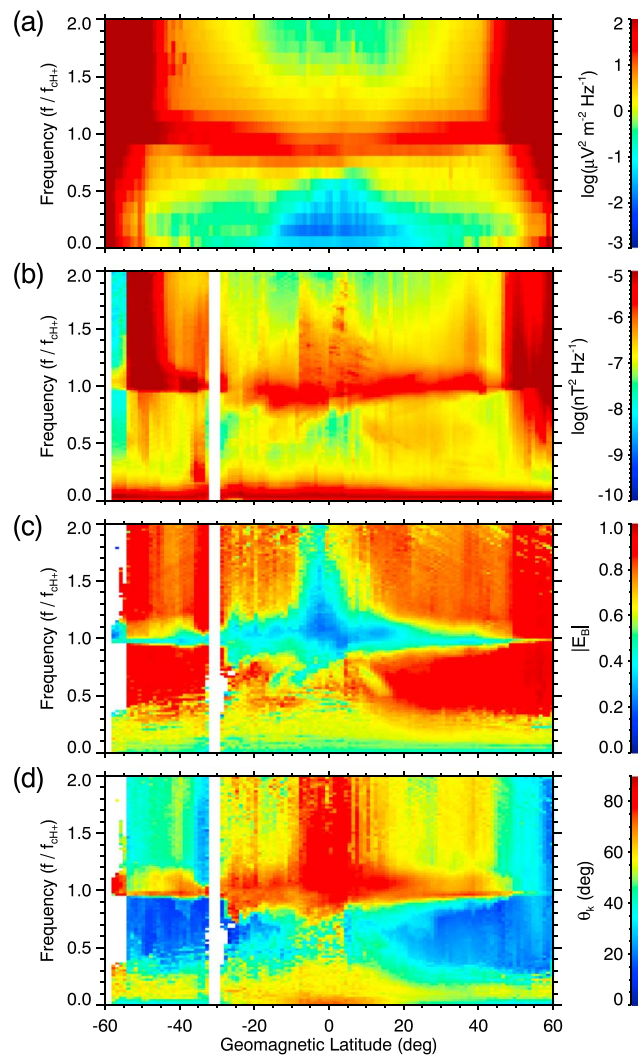


**Figure 7.** Analogous to Figure 4 but superposed for all six analyzed geomagnetic storms. The data obtained within 2 days after the individual *Dst* minima were used.

several days, until eventually reaching low prestorm levels toward the end of the plotted time interval. During the nighttime (Figure 5d), there is a smaller increase of the wave intensity at lower frequencies, just after the time of the *Dst* minimum. We note that this general evolution trend is confirmed also when checking all the six geomagnetic storms individually (not shown).

Average wave propagation parameters within 5° from the geomagnetic equator are analyzed in Figure 6. Again, the used format is analogous to that of Figure 3, but this time the data from all the six geomagnetic storms are included. Only the dayside data were used. The values of ellipticity are close to 0 principally during all the analyzed frequency-time interval with increased wave intensity. This means that the waves are nearly linearly polarized, as is expected for EN emissions. The values of polar angle of wave vector direction are close to 90°, corresponding to the wave vector perpendicular to the ambient magnetic field. We note that this picture of the wave propagation properties is confirmed also when checking the propagation properties observed during each analyzed geomagnetic storm separately (not shown).

The results obtained using the superposed epoch analysis are shown in Figure 7 using the normalized frequency-geomagnetic latitude representation. The format of the figure is analogous to that of Figure 4. Again, the data obtained within 2 days after the individual *Dst* minima were used. One can identify two regions of increased wave intensity at larger geomagnetic latitudes. These are, however, not relevant for the present study, as we focus on the emissions in the equatorial region. There, the increased wave intensity is limited to

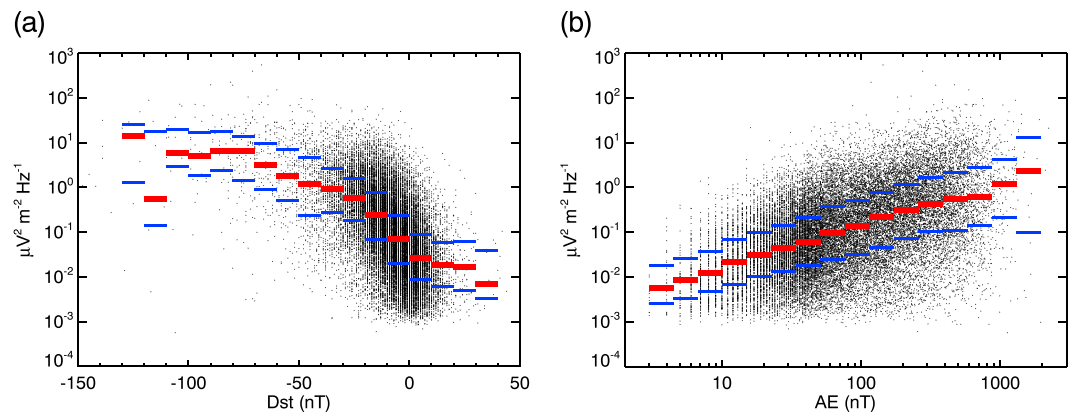


**Figure 8.** (a) Mean daytime power spectral density of electric field fluctuations at the proton cyclotron frequency within  $5^\circ$  from the geomagnetic equator as a function of  $Dst$  index. The red horizontal lines correspond to median values of power spectral density in given intervals of  $Dst$  index. The blue horizontal lines correspond to 0.25 and 0.75 quartiles of power spectral density in given intervals of  $Dst$  index. (b) Same as Figure 8a but for  $AE$  index.

frequencies larger than the proton cyclotron frequency (or, more precisely, to frequencies larger than the  $L = 0$  cutoff which is slightly lower than the proton cyclotron frequency). The emissions in this frequency-latitude region are nearly linearly polarized, and they have wave vectors almost perpendicular to the ambient Earth's magnetic field; i.e., their propagation properties correspond to those expected for EN emissions.

The importance of enhanced geomagnetic activity for the occurrence of increased wave intensity in the equatorial region at DEMETER altitudes is further demonstrated in Figure 8. This time the analysis is not limited to specific storm time intervals, and the data measured during all DEMETER dayside half-orbits are used instead. Following the aforementioned results of the wave intensity being increased primarily at frequencies around the proton cyclotron frequency, we focused on the region of geomagnetic latitudes within  $5^\circ$  from the geomagnetic equator and frequency bins of the VLF Survey mode data corresponding to the proton cyclotron frequency at the spacecraft location. Resulting mean power spectral density of electric field fluctuations calculated for each daytime equatorial crossing of the DEMETER spacecraft is then plotted as a function of  $Dst$  and  $AE$  indices in Figures 8a and 8b, respectively. The red horizontal lines correspond to mean power spectral densities of electric field fluctuations in given  $Dst/AE$  intervals. The blue horizontal lines correspond to 0.25 and 0.75 quartiles. It can be seen that the wave intensity systematically increases with decreasing  $Dst$  index and with increasing  $AE$  index. The values of Spearman rank correlation coefficients [Sheskin, 2011] obtained for  $Dst/AE$  index dependencies are about  $-0.54$  and  $0.45$ , respectively. The variation of the wave intensity is indeed rather dramatic, as large as about 3 orders of magnitude.

#### 4. Discussion

A possible propagation of EN emissions down to low altitudes was formerly investigated using a simplified theoretical analysis, suggesting that it is indeed possible when the wave vector lies very close to the meridional plane, i.e., when it has a negligible azimuthal component [Chen and Thorne, 2012]. Santolik *et al.* [2016] presented a case study of such an event, combining 3-D ray tracing calculations and a detailed wave analysis of DEMETER data. They demonstrated the importance of multi-ion plasma composition at DEMETER altitudes and the resulting lower frequency ( $L = 0$ ) cutoff of the emissions observed by DEMETER. The  $L = 0$  cutoff frequency depends on the plasma composition, and it is lower than the proton cyclotron frequency. Its existence is crucial also for the results presented in this study.

As waves at frequencies above the  $L = 0$  cutoff should be able to penetrate down to DEMETER altitudes, upper frequencies of observed EN emissions likely correspond to upper frequencies of EN emissions in the generation region. Given that EN propagates in the extraordinary mode nearly perpendicular to the ambient Earth's magnetic field, these frequencies should be lower than the lower hybrid frequency in the source region. EN emissions observed by DEMETER typically extend to frequencies up to about 600–800 Hz (see Figure 6). In the dense plasma approximation, the lower hybrid frequency is equal to the harmonic average of proton and electron cyclotron frequencies; i.e., it is equal to about 42.85 times the proton cyclotron frequency. Using a

dipole approximation for the magnetic field magnitude, we can thus obtain an upper estimate of the radial distance where EN observed by DEMETER is generated, about  $2.9\text{--}3.2 R_E$ , roughly consistent with estimates of Santolik *et al.* [2016] based on the line structure observed in the high-resolution Burst mode data.

As EN emissions are believed to be generated at multiples of proton cyclotron frequency in the source region, the frequencies of individual observed lines should correspond to the harmonics of the proton cyclotron frequency in the source region. The frequency separation of consecutive lines would then give us the ion cyclotron frequency in the source [Posch *et al.*, 2015; Santolik *et al.*, 2016]. Nevertheless, this approach is somewhat difficult to apply routinely to DEMETER data. The reason is that the observed line structure is usually so complex that it is difficult to identify a clear harmonic line structure. This is probably due to emissions coming from various radial distances being observed at the same time, which results in overlapping of many individual harmonic line systems.

The wave data measured by DEMETER during six strong isolated geomagnetic storms demonstrate that the occurrence of EN emissions during the storm periods is a systematic phenomenon. Although at other times the wave intensity at geomagnetic equator is usually rather low, during disturbed periods and at frequencies between the  $L = 0$  cutoff frequency and about 600–800 Hz EN emissions are intense and dominant. There may be two principal reasons that the increased geomagnetic activity is so crucial for EN emissions to be observed by DEMETER. First, as suggested by Santolik *et al.* [2016], the intensity of EN emissions observed at larger radial distances generally increases with the geomagnetic activity [Meredith *et al.*, 2008; Ma *et al.*, 2013; Hrbáčková *et al.*, 2015; Němec *et al.*, 2015a]. More intense emissions are more likely to penetrate to DEMETER altitudes with significant intensities. This scenario is consistent with the observed EN intensities at DEMETER altitudes increasing with the geomagnetic activity. However, a comparison of the results depicted in Figure 8 with the results from Figure 5 of Němec *et al.* [2015a] suggests that the intensity of EN emissions at low altitudes might increase with the geomagnetic activity more significantly than the intensity of EN emissions at larger radial distances. If this is really the case, it might indicate a possible change of the radial distance of EN generation region during periods of enhanced geomagnetic activity. Specifically, if the generation region of EN emissions moved to lower radial distances at the times of larger geomagnetic activity, the penetration of the emissions down to DEMETER altitudes at these times would be easier. Moreover, the lower hybrid frequency in the generation region would be higher, and the frequency bandwidth of the emissions reaching DEMETER could be thus larger.

As for the geomagnetic latitudes where EN emissions are observed on DEMETER, the results from Figure 7 show that the emissions extend to latitudes as large as about  $20^\circ$ . The latitudinal extent appears to be larger at lower frequencies. This could be due to the frequency spectrum of EN emissions at DEMETER. As EN emissions on DEMETER principally always extend down to low frequencies, but their occurrence at higher frequencies might be sporadic, at higher frequencies they are likely mixed with other emissions, resulting in apparently lower latitudinal extent. This frequency spectrum of observed EN emissions is consistent with ray tracing results by Santolik *et al.* [2016], who found that lower frequency waves penetrate easier to low altitudes.

Finally, it is curious that EN emissions observed by DEMETER are dominant during the daytime, while they are much weaker during the night. This is rather a different pattern than observed at larger radial distances. There, although EN emissions occur more often during the day than during the night [Green *et al.*, 2005; Ma *et al.*, 2013], the difference is far less striking, in particular inside the plasmasphere [Hrbáčková *et al.*, 2015; Němec *et al.*, 2015a]. This might possibly indicate that during geomagnetic storms, the source region of EN emissions is located at lower radial distances and preferably on the dayside. This could be consistent with the strong day-night asymmetry of the Earth's magnetic field under disturbed geomagnetic conditions, and with the plasmasphere possibly being more compressed on the dayside than on the nightside during these periods [Moldwin *et al.*, 2002].

## 5. Conclusions

We analyzed electromagnetic wave data measured by the DEMETER spacecraft during six strong ( $Dst < -100$  nT) isolated geomagnetic storms which occurred during the mission lifetime and for which the data were available. We have shown, both using a selected event and using a superposed epoch analysis, that the daytime wave intensity in the equatorial region is significantly increased during the storm periods at frequencies above the  $L = 0$  cutoff. Only a small wave intensity increase was observed during the nighttime. Multicomponent wave measurements performed during the Burst mode allowed us to perform a detailed

wave analysis. It was found that the waves are nearly linearly polarized, with wave vectors almost perpendicular to the ambient Earth's magnetic field, as it has been previously demonstrated for EN emissions penetrating down to the altitudes of the DEMETER spacecraft (at a radial distance of about  $1.1R_E$ ). Finally, we used the data from all daytime equatorial crossings of the spacecraft to obtain a dependence of the wave intensity at the proton cyclotron frequency in the equatorial region on *Dst* and *AE* geomagnetic indices. We demonstrated that the wave intensity increases by as much as 3 orders of magnitude during geomagnetically disturbed periods. The obtained results show that during geomagnetically disturbed conditions, the EN emissions penetrate to very low altitudes and eventually become the most important daytime emission in a given range of frequencies and latitudes.

#### Acknowledgments

DEMETER was a CNES mission. We thank the engineers from CNES and scientific laboratories (CBK, IRAP, LPC2E, LPP, and SSD of ESTEC) who largely contributed to the success of this mission. DEMETER data are accessible from <https://sipad-cdpp.cnes.fr>. *Dst* and *AE* indices can be downloaded from the World Data Center for Geomagnetism, Kyoto (<http://wdc.kugi.kyoto-u.ac.jp/dstae/index.html>). The work of F.N. was supported by GACR grant 15-01775Y. The work of O.S. was supported by MSMT grant LH 15304, GACR grant 14-31899S, and by the Praemium Academiae award from the CAS.

#### References

- Balikhin, M. A., Y. Y. Shprits, S. N. Walker, L. Chen, N. Cornilleau-Wehrin, I. Dandouras, O. Santolík, C. Carr, K. H. Yearby, and B. Weiss (2015), Observations of discrete harmonics emerging from equatorial noise, *Nat. Commun.*, *6*, 7703, doi:10.1038/ncomms8703.
- Berthelier, J. J., et al. (2006), ICE, the electric field experiment on DEMETER, *Planet. Space Sci.*, *54*, 456–471.
- Berthelier, J.-J., M. Malingre, R. Pfaff, E. Seran, R. Pottelette, J. Jasperse, J.-P. Lebreton, and M. Parrot (2008), Lightning-induced plasma turbulence and ion heating in equatorial ionospheric depletions, *Nat. Geosci.*, *1*, 101–105, doi:10.1038/ngeo109.
- Boardsen, S. A., D. L. Gallagher, D. A. Gurnett, W. K. Peterson, and J. L. Green (1992), Funnel-shaped, low-frequency equatorial waves, *J. Geophys. Res.*, *97*, 14,967–14,976.
- Boardsen, S. A., G. B. Hospodarsky, C. A. Kletzing, R. F. Pfaff, W. S. Kurth, J. R. Wygant, and E. A. MacDonald (2014), Van Allen Probe observations of periodic rising frequencies of the fast magnetosonic mode, *Geophys. Res. Lett.*, *41*, 8161–8168, doi:10.1002/2014GL062020.
- Boardsen, S. A., et al. (2016), Survey of the frequency dependent latitudinal distribution of the fast magnetosonic wave mode from Van Allen Probes Electric and Magnetic Field Instrument and Integrated Science waveform receiver plasma wave analysis, *J. Geophys. Res. Space Physics*, *121*, 2902–2921, doi:10.1002/2015JA021844.
- Bortnik, J., and R. M. Thorne (2010), Transit time scattering of energetic electrons due to equatorially confined magnetosonic waves, *J. Geophys. Res.*, *115*, A07213, doi:10.1029/2010JA015283.
- Bortnik, J., R. M. Thorne, B. Ni, and J. Li (2015), Analytical approximation of transit time scattering due to magnetosonic waves, *Geophys. Res. Lett.*, *42*, 1318–1325, doi:10.1002/2014GL062710.
- Broughton, M. C., J. LaBelle, and M. Parrot (2014), DEMETER observations of bursty MF emissions and their relation to ground-level auroral MF burst, *J. Geophys. Res. Space Physics*, *119*, 10,144–10,155, doi:10.1002/2014JA020410.
- Chen, L., and R. M. Thorne (2012), Perpendicular propagation of magnetosonic waves, *Geophys. Res. Lett.*, *39*, L14102, doi:10.1029/2012GL052485.
- Chen, L., R. M. Thorne, V. K. Jordanova, M. F. Thomsen, and R. B. Horne (2011), Magnetosonic wave instability analysis for proton ring distributions observed by the LANL magnetospheric plasma analyzer, *J. Geophys. Res.*, *116*, A03223, doi:10.1029/2010JA016068.
- Chen, L., J. Sun, Q. Lu, X. Gao, Z. Xia, and Z. Zhima (2016), Generation of magnetosonic waves over a continuous spectrum, *J. Geophys. Res. Space Physics*, *121*, 1137–1147, doi:10.1002/2015JA022089.
- Colpitts, C. A., C. A. Cattell, J. U. Kozyra, and M. Parrot (2012), Satellite observations of banded VLF emissions in conjunction with energy-banded ions during very large geomagnetic storms, *J. Geophys. Res.*, *117*, A10211, doi:10.1029/2011JA017329.
- Fu, H. S., J. B. Cao, Z. Zhima, Y. V. Khotyaintsev, V. Angelopoulos, O. Santolík, Y. Omura, U. Taubenschuss, L. Chen, and S. Y. Huang (2014), First observation of rising-tone magnetosonic waves, *Geophys. Res. Lett.*, *41*, 7419–7426, doi:10.1002/2014GL061867.
- Green, J. L., S. Boardsen, L. Garcia, W. W. L. Taylor, S. F. Fung, and B. W. Reinisch (2005), On the origin of whistler mode radiation in the plasmasphere, *J. Geophys. Res.*, *110*, A03201, doi:10.1029/2004JA010495.
- Gurnett, D. A. (1976), Plasma wave interactions with energetic ions near the magnetic equator, *J. Geophys. Res.*, *81*, 2765–2770.
- Gurnett, D. A., and T. B. Burns (1968), The low-frequency cutoff of ELF emissions, *J. Geophys. Res.*, *73*(23), 7437–7445.
- Hayosh, M., D. L. Pasmanik, A. G. Demekhov, O. Santolík, M. Parrot, and E. E. Titova (2013), Simultaneous observations of quasi-periodic ELF/VLF wave emissions and electron precipitation by DEMETER satellite: A case study, *J. Geophys. Res. Space Physics*, *118*, 4523–4533, doi:10.1002/jgra.50179.
- Hayosh, M., F. Němec, O. Santolík, and M. Parrot (2014), Statistical investigation of VLF quasiperiodic emissions measured by the demeter spacecraft, *J. Geophys. Res. Space Physics*, *119*, 8063–8072, doi:10.1002/2013JA019731.
- Hayosh, M., F. Němec, O. Santolík, and M. Parrot (2016), Propagation properties of quasiperiodic VLF emissions observed by the DEMETER spacecraft, *Geophys. Res. Lett.*, *43*, 1007–1014, doi:10.1002/2015GL067373.
- Horne, R. B., G. V. Wheeler, and H. S. C. Alleyne (2000), Proton and electron heating by radially propagating fast magnetosonic waves, *J. Geophys. Res.*, *105*(A12), 27,597–27,610.
- Horne, R. B., R. M. Thorne, S. A. Glauert, N. P. Meredith, D. Pokhotelov, and O. Santolík (2007), Electron acceleration in the Van Allen radiation belts by fast magnetosonic waves, *J. Geophys. Res.*, *34*, L17107, doi:10.1029/2007GL030267.
- Hrbáčková, Z., O. Santolík, F. Němec, E. Macúšová, and N. Cornilleau-Wehrin (2015), Systematic analysis of occurrence of equatorial noise emissions using 10 years of data from the Cluster mission, *J. Geophys. Res. Space Physics*, *120*, 1007–1021, doi:10.1002/2014JA020268.
- Kasahara, Y., H. Kenmochi, and I. Kimura (1994), Propagation characteristics of the ELF emissions observed by the satellite Akebono in the equatorial plane, *Radio Sci.*, *29*, 751–767.
- Laakso, H., H. Junginger, A. Roux, R. Schmidt, and C. de Villedary (1990), Magnetosonic waves above  $f_{CH+}$  at geostationary orbit: GEOS 2 results, *J. Geophys. Res.*, *95*, 10,609–10,621.
- Liu, K., S. P. Gary, and D. Winske (2011), Excitation of magnetosonic waves in the terrestrial magnetosphere: Particle-in-cell simulations, *J. Geophys. Res.*, *116*, A07212, doi:10.1029/2010JA016372.
- Ma, Q., W. Li, R. M. Thorne, and V. Angelopoulos (2013), Global distribution of equatorial magnetosonic waves observed by THEMIS, *Geophys. Res. Lett.*, *40*, 1895–1901, doi:10.1002/grl.50434.
- Ma, Q., W. Li, L. Chen, R. M. Thorne, and V. Angelopoulos (2014), Magnetosonic wave excitation by ion ring distributions in the Earth's inner magnetosphere, *J. Geophys. Res. Space Physics*, *119*, 844–852, doi:10.1002/2013JA019591.
- Ma, Q., W. Li, R. M. Thorne, J. Bortnik, C. A. Kletzing, W. S. Kurth, and G. B. Hospodarsky (2016), Electron scattering by magnetosonic waves in the inner magnetosphere, *J. Geophys. Res. Space Physics*, *121*, 274–285, doi:10.1002/2015JA021992.

- Malingre, M., J.-J. Berthelier, R. Pfaff, J. Jasperse, and M. Parrot (2008), Lightning-induced lower-hybrid turbulence and trapped extremely low frequency (ELF) electromagnetic waves observed in deep equatorial plasma density depletions during intense magnetic storms, *J. Geophys. Res.*, *113*, A11320, doi:10.1029/2008JA013463.
- McClements, K. G., R. O. Dendy, and C. N. Lashmore-Davis (1994), A model for the generation of obliquely propagating ULF waves near the magnetic equator, *J. Geophys. Res.*, *99*, 23,685–23,693.
- Menk, F. W. (2011), Magnetospheric ULF waves: A review, in *The Dynamic Magnetosphere, IAGA Spec. Sopron Book Ser.*, vol. 3, edited by W. Liu and M. Fujimoto, pp. 223–256, Springer, Netherlands, doi:10.1007/978-94-007-0501-2\_13.
- Meredith, N. P., R. B. Horne, and R. R. Anderson (2008), Survey of magnetosonic waves and proton ring distributions in the Earth's inner magnetosphere, *J. Geophys. Res.*, *113*, A06213, doi:10.1029/2007JA012975.
- Moldwin, M. B., L. Downward, H. K. Rassoul, R. Amin, and R. R. Anderson (2002), A new model of the location of the plasmopause: CRRES results, *J. Geophys. Res.*, *107*(A11), 1339, doi:10.1029/2001JA009211.
- Němec, F., O. Santolík, K. Gereová, E. Macúšová, Y. de Conchy, and N. Cornilleau-Wehrlin (2005), Initial results of a survey of equatorial noise emissions observed by the Cluster spacecraft, *Planet. Space Sci.*, *53*, 291–298.
- Němec, F., O. Santolík, M. Parrot, and C. J. Rodger (2010), Relationship between median intensities of electromagnetic emissions in the VLF range and lightning activity, *J. Geophys. Res.*, *115*, A08315, doi:10.1029/2010JA015296.
- Němec, F., O. Santolík, J. S. Pickett, Z. Hrbáčková, and N. Cornilleau-Wehrlin (2013), Azimuthal directions of equatorial noise propagation determined using 10 years of data from the Cluster spacecraft, *J. Geophys. Res. Space Physics*, *118*, 7160–7169, doi:10.1002/2013JA019373.
- Němec, F., O. Santolík, Z. Hrbáčková, and N. Cornilleau-Wehrlin (2015a), Intensities and spatiotemporal variability of equatorial noise emissions observed by the Cluster spacecraft, *J. Geophys. Res. Space Physics*, *120*, 1620–1632, doi:10.1002/2014JA020814.
- Němec, F., O. Santolík, Z. Hrbáčková, J. S. Pickett, and N. Cornilleau-Wehrlin (2015b), Equatorial noise emissions with quasiperiodic modulation of wave intensity, *J. Geophys. Res. Space Physics*, *120*, 2649–2661, doi:10.1002/2014JA020816.
- Parrot, M., and J.-J. Berthelier (2012), AKR-like emissions observed at low altitude by the DEMETER satellite, *J. Geophys. Res.*, *117*, A10314, doi:10.1029/2012JA017937.
- Parrot, M., et al. (2006a), The magnetic field experiment IMSC and its data processing onboard DEMETER: Scientific objectives, description and first results, *Planet. Space Sci.*, *54*, 441–455.
- Parrot, M., A. Buzzi, O. Santolík, J. J. Berthelier, J. A. Sauvaud, and J. P. Lebreton (2006b), New observations of electromagnetic harmonic ELF emissions in the ionosphere by the DEMETER satellite during large magnetic storms, *J. Geophys. Res.*, *111*, A08301, doi:10.1029/2005JA011583.
- Parrot, M., F. Němec, and O. Santolík (2014), Analysis of fine ELF wave structures observed poleward from the ionospheric trough by the low-altitude satellite DEMETER, *J. Geophys. Res. Space Physics*, *119*, 2052–2060, doi:10.1002/2013JA019557.
- Perraut, S., A. Roux, P. Robert, R. Gendrin, J. A. Sauvaud, J. M. Bosqued, G. Kremser, and A. Korth (1982), A systematic study of ULF waves above  $f_{H+}$  from GEOS 1 and 2 measurements and their relationships with proton ring distributions, *J. Geophys. Res.*, *87*, 6219–6236.
- Píša, D., M. Parrot, O. Santolík, and J. D. Menietti (2015), EMIC waves observed by the low-altitude satellite DEMETER during the November 2004 magnetic storm, *J. Geophys. Res. Space Physics*, *120*, 5455–5464, doi:10.1002/2014JA020233.
- Posch, J. L., M. J. Engebretson, C. N. Olson, S. A. Thaller, A. W. Breneman, J. R. Wygant, S. A. Boardsen, C. A. Kletzing, C. W. Smith, and G. D. Reeves (2015), Low-harmonic magnetosonic waves observed by the Van Allen Probes, *J. Geophys. Res. Space Physics*, *120*, 6230–6257, doi:10.1002/2015JA021179.
- Russell, C. T., R. E. Holzer, and E. J. Smith (1970), OGO 3 observations of ELF noise in the magnetosphere. The nature of the equatorial noise, *J. Geophys. Res.*, *75*(4), 755–768.
- Santolík, O., J. S. Pickett, D. A. Gurnett, M. Maksimovic, and N. Cornilleau-Wehrlin (2002), Spatiotemporal variability and propagation of equatorial noise observed by Cluster, *J. Geophys. Res.*, *107*(A12), 1495, doi:10.1029/2001JA009159.
- Santolík, O., M. Parrot, and F. Lefeuvre (2003), Singular value decomposition methods for wave propagation analysis, *Radio Sci.*, *38*(1), 1010, doi:10.1029/2000RS002523.
- Santolík, O., F. Němec, K. Gereová, E. Macúšová, Y. de Conchy, and N. Cornilleau-Wehrlin (2004), Systematic analysis of equatorial noise below the lower hybrid frequency, *Ann. Geophys.*, *22*, 2587–2595.
- Santolík, O., F. Němec, M. Parrot, D. Lagoutte, L. Madrias, and J. J. Berthelier (2006), Analysis methods for multi-component wave measurements on board the DEMETER spacecraft, *Planet. Space Sci.*, *54*, 512–527.
- Santolík, O., M. Parrot, and F. Němec (2016), Propagation of equatorial noise to low altitudes: Decoupling from the magnetosonic mode, *Geophys. Res. Lett.*, *43*, 6694–6704, doi:10.1002/2016GL069582.
- Sheskin, D. J. (2011), *Handbook of Parametric and Nonparametric Statistical Procedures*, 5th ed., CRC Press, Boca Raton, Fla.
- Shprits, Y. Y. (2016), Estimation of bounce resonance scattering by fast magnetosonic waves, *Geophys. Res. Lett.*, *43*, 998–1006, doi:10.1002/2015GL066796.
- Stix, T. H. (1992), *Waves in Plasmas*, chap. Wave normal surfaces, waves in a cold uniform plasma, pp. 1–46, Springer, New York.
- Tsurutani, B., B. J. Falkowski, J. S. Pickett, O. P. Verkhoglyadova, O. Santolík, and G. S. Lakhina (2014), Extremely intense ELF magnetosonic waves: A survey of polar observations, *J. Geophys. Res. Space Physics*, *119*, 964–977, doi:10.1002/2013JA019284.
- Walker, S. N., M. A. Balikhin, D. R. Shklyar, K. H. Yearby, P. Canu, C. M. Carr, and I. Dandouras (2015), Experimental determination of the dispersion relation of magnetosonic waves, *J. Geophys. Res. Space Physics*, *120*, 9632–9650, doi:10.1002/2015JA021746.
- Xiao, F., Q. Zhou, Z. He, and L. Tang (2012), Three-dimensional ray tracing of fast magnetosonic waves, *J. Geophys. Res.*, *117*, A06208, doi:10.1029/2012JA017589.
- Xiao, F., Q. Zhou, Z. He, C. Yang, Y. He, and L. Tang (2013), Magnetosonic wave instability by proton ring distributions: Simultaneous data and modeling, *J. Geophys. Res. Space Physics*, *118*, 4053–4058, doi:10.1002/jgra.50401.
- Zhima, Z., J. B. Cao, W. L. Liu, H. S. Fu, T. Y. Wang, and X. M. Zhang (2014), Storm time evolution of ELF/VLF waves observed by DEMETER satellite, *J. Geophys. Res. Space Physics*, *119*, 2612–2622, doi:10.1002/2013JA019237.
- Zhima, Z., L. Chen, H. Fu, J. Cao, R. B. Horne, and G. Reeves (2015), Observations of discrete magnetosonic waves off the magnetic equator, *Geophys. Res. Lett.*, *42*, 9694–9701, doi:10.1002/2015GL066255.